

# SaliencyCut: Augmenting Plausible Anomalies for Open-set Fine-Grained Anomaly Detection

Jianan Ye<sup>1,2,\*</sup>, Yijie Hu<sup>1,2,\*</sup>, Xi Yang<sup>1</sup>, Qiu-Feng Wang<sup>1</sup>, Chao Huang<sup>3</sup>, Kaizhu Huang<sup>4,†</sup>

<sup>1</sup>School of Advanced Technology, Xi'an Jiaotong-Liverpool University

<sup>2</sup>Department of Electrical Engineering and Electronics, University of Liverpool

<sup>3</sup>Department of Computer Science, University of Liverpool

<sup>4</sup>Data Science Research Center, Duke Kunshan University

{Jianan.Ye20, Yijie.Hu20}@student.xjtlu.edu.cn, {Xi.Yang01, Qiufeng.Wang}@xjtlu.edu.cn,  
Chao.Huang2@liverpool.ac.uk, kaizhu.huang@dukekunshan.edu.cn

## Abstract

Open-set fine-grained anomaly detection is a challenging task that requires learning discriminative fine-grained features to detect anomalies that were even unseen during training. As a cheap yet effective approach, data augmentation has been widely used to create pseudo anomalies for better training of such models. Recent wisdom of augmentation methods focuses on generating random pseudo instances that may lead to a mixture of augmented instances with seen anomalies, or out of the typical range of anomalies. To address this issue, we propose a novel saliency-guided data augmentation method, SaliencyCut, to produce pseudo but more common anomalies which tend to stay in the plausible range of anomalies. Furthermore, we deploy a two-head learning strategy consisting of normal and anomaly learning heads, to learn the anomaly score of each sample. Theoretical analyses show that this mechanism offers a more tractable and tighter lower bound of the data log-likelihood. We then design a novel patch-wise residual module in the anomaly learning head to extract and assess the fine-grained anomaly features from each sample, facilitating the learning of discriminative representations of anomaly instances. Extensive experiments conducted on six real-world anomaly detection datasets demonstrate the superiority of our method to the baseline and other state-of-the-art methods under various settings.

## 1. Introduction

Fined-grained anomaly detection is designed to detect defective samples that exhibit minor deviations from ex-

\*Equal contribution.

†Corresponding author.

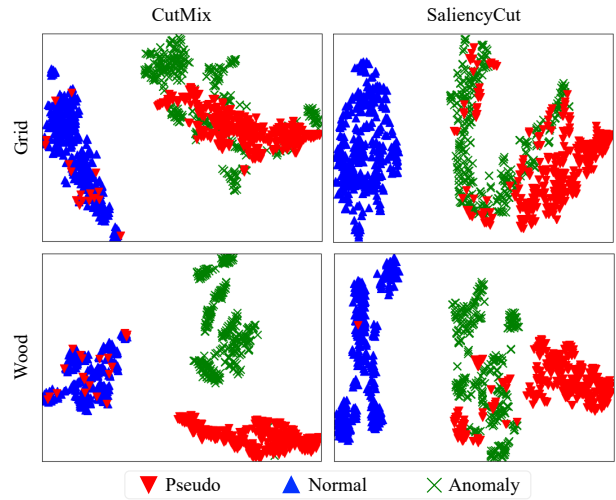


Figure 1. t-SNE visualizations of data distribution in the feature space during training on two datasets. Pseudo anomaly samples are created by CutMix [48] in a random way which tend to be mixed with both seen anomalous and normal samples, or overly expand the training anomaly samples (red triangles in left-bottom). Our method migrates these issues.

pected data patterns yet share similarities with the primary patterns of normal samples [19, 7, 27, 26]. Unlike conventional open-set or out-of-distribution methods [21, 44, 1, 49, 39], open-set fine-grained anomaly detection targets both seen (e.g., color spots on leather surfaces) and unseen types of anomalies (e.g., folds or glues on leather surfaces) within a single object class during training. To deal with this open-set problem, it is crucial for the detection model to have the ability to identify both seen and unseen types of anomalies. Retraining the model every time new anomaly data appears is a straightforward solution, but it can be inefficient and costly. Additionally, even for seen anomalies, there may be

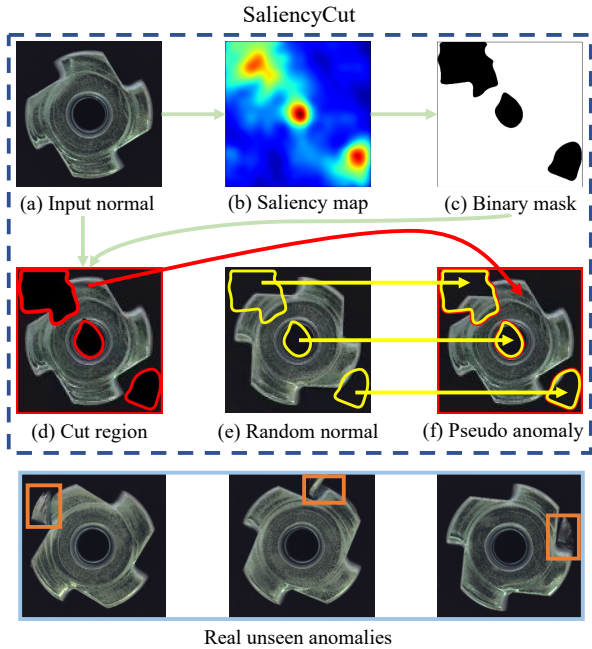


Figure 2. Illustration of SaliencyCut for generating pseudo anomalies. Real unseen anomalies are shown in the last low, anomaly regions are marked with orange boxes. The resulting pseudo anomaly looks very similar to real unseen anomalies.

a scarcity of available samples, which makes this problem even more challenging.

Given that anomalies are akin to normal samples, adding perturbation is one cheapest way to expand anomalies distribution for tackling open-set fine-grained anomaly detection. Current efforts [7, 19] focus on creating pseudo instances by data augmentation methods like CutMix [48] or CutPaste [19]. By simulating the possible types of unseen instances, more diverse pseudo anomalies are involved during training to learn rich discriminative anomaly features. However, lacking the guidance of real anomaly information, such methods usually synthesize pseudo instances in a random way. As a result, the pseudo anomalies could either overlap with the distribution of the seen training instances or unduly expand the distribution of the anomalies. Figure 1 illustrates one simple example. In the left part, Cutmix, one typical data augmentation method generates pseudo anomaly instances that are mixed with both seen normal and anomaly instances in Grid data (left-top of Figure 1). For the Wood data (left-bottom of Figure 1), it is evident that the pseudo instances unduly expand the distribution of the anomalies. Obviously, pseudo anomalies either mixed with the existing samples or staying too farther away from anomalies may confuse the detection model and thus limit the performance.

In this paper, we argue that one ideal anomaly-data augmentation method should generate samples that are neither

far away nor mixed with seen anomalies. Moreover, it is observed that salient regions of normal instances representing the typical normal regions would be essentially more likely to be recognized as normal instances instead of anomalies, while non-salient regions could have a higher chance to contain anomaly information. Motivated by these observations, we present a novel saliency-guided data augmentation method called *SaliencyCut* to mitigate the defects of random pseudo-anomalies generation methods (e.g., CutMix or CutPaste), i.e., we aim to generate pseudo anomaly data guided by saliency so that they would not be mixed with normal instances but tend to stay in the plausible range of anomalies. To do so, 1) we first obtain the saliency map of a normal instance by calculating the backward propagated gradients, thus the saliency part would stand for more typical or reliable normal instance regions; 2) we then cut the non-salient regions from the normal instance, and paste them to any other random normal instance to obtain a final pseudo anomaly. See Figure 2 for the detailed flowchart of our SaliencyCut. While the saliency region generally indicates the more reliable or confident part as a normal instance, the non-salient parts would tend to stay farther from a normal instance. Namely, they have a higher chance to distribute closer to anomalies. By mixing such non-salient regions, the resulting pseudo instances tend to stay closer to the anomalies and would be less likely to overlap with normal instances. As clearly illustrated in Figure 1, in the right part, pseudo instances generated by our SaliencyCut are indeed rarely mixed with normal instances and also expand the plausible region of anomalies. As also observed in the last two rows of Figure 2, the resulting augmented sample (f) looks much similar to the real anomalies (last row).

On the implementation front, in order to enable the model to further discriminate against all types of anomalies with SaliencyCut, we design a novel two-head learning mechanism to learn the score distribution of normal and anomalous samples. One head focuses on learning the features of normal samples, while the other focuses on learning fine-grained anomaly features through anomalous residuals within extracted features, thus promoting the model to discriminate against anomalous samples. To efficiently learn such anomalous residuals, we propose one patch-wise residual module, where residual features within each sample are calculated for enlarging the gap between normal and anomaly samples. As a result, our model learns abnormality representations, which can discriminate both seen and unseen anomalies from the normal data, as shown in Figure 6. As an important contribution, we have provided theoretical analysis showing that our two-head learning mechanism offers on the data log-likelihood a tighter lower bound than the four-head approach [7] that is more tractable to optimize, thus justifying our novel framework.

We summarize our contributions as follows: 1) We pro-

pose a saliency-guided data augmentation, namely SaliencyCut, creating pseudo anomalies to expand the range of anomaly samples, improving the model’s detection ability on unseen anomalies. 2) We deploy a two-head learning mechanism based on the theoretical lower bound in the anomaly score learning process. 3) We further design a novel patch-wise residual module to gather fine-grained anomaly knowledge. 4) We conduct comprehensive experiments on six real application datasets. Experimental results show that our model substantially outperforms state-of-the-art competing models in various settings.

## 2. Related Work

**Open-set/Out-of-Distribution Detection.** Open-set detection and out-of-distribution detection are recognized as coarser-grained detection methods. Open-set detection [21, 44, 1, 54, 47] seeks to identify novel object classes that were not accounted for during training, and out-of-distribution detection [16, 20, 49, 39] seeks to detect data that is significantly dissimilar from the training data. Our task, on the other hand, is oriented towards fine-grained detection, with the aim of identifying subtle anomaly characteristics in samples of a single object within an open-set scenario.

**Supervised Anomaly Detection Methods.** In recent years, supervised anomaly detection attracts increasing attention, which aims to enhance the ability of deep learning models to identify anomaly samples by learning anomaly features from a small number of seen anomalies. One-class metric learning framework [11, 22, 25, 33] with anomalies as negative samples or models learning with deviation loss [27, 52, 26] are proposed to tackle this issue. As these methods introduce anomaly samples into the training process, a consequent problem is that the models overfit the seen types of anomalies.

**Anomaly-Free Detection Methods.** By assuming that anomaly samples are not available during the training stage, considerable progress has been made in anomaly-free detection studies under the one-classification framework [4, 5, 30, 32], self-supervised framework [2, 8, 9, 19, 38, 42, 45], GAN-based framework [29, 34, 36, 50], and autoencoder-based framework [10, 14, 28, 53, 55]. Despite the fact that they do not suffer the danger of favoring the observed anomalies, it is challenging to distinguish anomaly samples from normal samples due to a lack of real anomalies.

**Augmentations.** Mixup [51] and CutMix [48] are two early augmentation methods that mix samples and labels, where the mixed samples are fed into networks as new data, and their corresponding labels are the mixed labels. Similar to CutMix, CutPaste [19] extracts a rectangular image patch of variable sizes from a normal image, rotates or jitters pixels in the patch, and pastes it back to an image at a random location. In the same way as CutPaste, DRA [7] employs CutMix to generate pseudo anomaly samples from normal

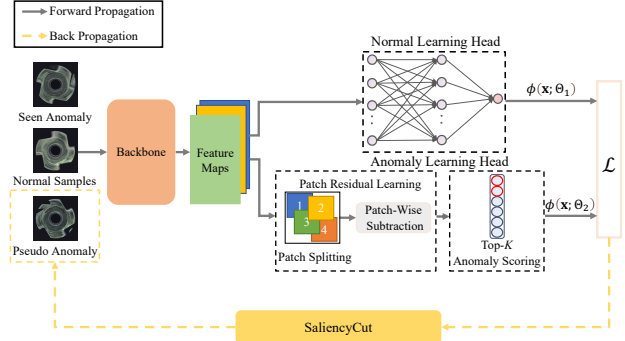


Figure 3. Overview of our proposed framework.

samples to be trained as a third class of samples in addition to normal and anomaly. Saliency-based data augmentation techniques such as SaliencyMix [43] and SAGE [24] use saliency regions to improve generalization for classification tasks by using saliency regions for CutMix [48] or overall saliency maximization mixup, but also involve label mixing. Our method, SaliencyCut, expands the anomaly distribution by using non-saliency regions of normal samples without label mixing, where augmented samples are treated as pseudo anomalies for expanding anomaly distribution.

## 3. Methodology

### 3.1. Problem Statement

We denote the training anomaly dataset as  $\mathcal{D} = \{\mathbf{x}_i\}_{i=1}^{n+m}$  which consists of  $n$  labeled normal samples  $\{x_1, x_2 \dots x_n\}$  and  $m$  labeled anomaly samples  $\{x_{n+1}, x_{n+2} \dots x_{n+m}\}$  ( $n \gg m$ ). Here,  $m$  anomalies are from seen anomaly types  $\mathcal{S} \subset \mathcal{U}$ , where  $\mathcal{U} = \{c_i\}_{i=1}^{|\mathcal{U}|}$  denotes all types of anomalies. The goal is to learn an anomaly scoring network,  $\phi(\mathcal{D}) \rightarrow \mathbb{R}$ , which assigns larger anomaly scores to both sorts of anomalies (seen and unseen). We predict  $\phi(\mathbf{x}; \Theta_h)$ ,  $h \in \{1, 2\}$ , of two heads in the training phase, respectively, while performing  $\phi(\mathbf{x}; \Theta_2) - \phi(\mathbf{x}; \Theta_1)$  to obtain anomaly scores in inference.

### 3.2. Overview of Our Method

Our proposed method is composed of two major strategies: 1) we develop a data augmentation method that allows for the generation of pseudo but more plausible anomalies that tend to stay within a reasonable range of anomaly data; 2) we design a novel patch-wise residual module to gather anomaly knowledge and deploy a two-head learning strategy to learn the anomaly score of each sample, which effectively detects both seen and unseen anomalies.

The overall architecture is shown in Figure 3. We generate pseudo anomalies with SaliencyCut once before the beginning of each epoch in training, during which parameters of the network are not updated. In this phase, only nor-

---

**Algorithm 1: SaliencyCut Algorithm**

---

**Input:** Normal sample  $x_a$ , detection network  $f_\theta$ ,  
loss function  $\mathcal{L}$ .

**Output:** Pseudo Samples  $\tilde{x}$ .

- 1 Calculate gradients of  $Grad = \nabla_{x_a} \mathcal{L}(f_\theta(x_a))$ ;
  - 2 Saliency map  $G_a \leftarrow \text{normalize}(\text{smooth}(|Grad|))$ ;
  - 3 Saliency mask  $S_a = \text{threshold}(G_a)$ ;
  - 4 Randomly sample another normal instance  $x_b$ ;
  - 5 Pseudo sample  $\tilde{x} = (1 - S_a) \odot x_a + S_a \odot x_b$ ;
  - 6 **Return**  $\tilde{x}$
- 

mal and anomaly samples are fed into the network for forward propagation. The network’s gradients are then back-propagated according to the loss function. Saliency regions are calculated by the gradients of each pixel in normal samples, which are deployed by SaliencyCut to generate pseudo anomalies. Subsequently, training samples of normal, seen anomalies and pseudo anomalies are fed into the backbone network for feature extraction. Two scoring heads finally determine the anomaly score of each sample based on the extracted features. Normal Learning Head is constructed by 2-layers MLP. Anomaly Learning Head consists of a patch-wise residual module (in Section 3.5) and a top- $K$  anomaly scoring module [27, 26].

The network is optimized using the deviation loss [27, 26] in an end-to-end manner, which defines the deviation as a Z-score with Gaussian prior score:

$$\text{dev}(\mathbf{x}_i; \Theta_h) = \frac{\phi(\mathbf{x}_i; \Theta_h) - \mu_{\mathcal{R}}}{\sigma_{\mathcal{R}}}, h \in \{1, 2\}, \quad (1)$$

where  $\mu_{\mathcal{R}}$  and  $\sigma_{\mathcal{R}}$  represent the mean and standard deviation of prior-based anomaly score set drawn for Gaussian distribution. Then the deviation loss is specified by:

$$\mathcal{L} = \sum_{h=1,2} [(1 - y_i) |\text{dev}(\mathbf{x}_i; \Theta_h)| + y_i \max(0, a - \text{dev}(\mathbf{x}_i; \Theta_h))], \quad (2)$$

where  $y = 1$  if  $\mathbf{x}_i$  is an anomaly, and  $y = 0$  if  $\mathbf{x}_i$  is normal.  $a$  denotes a Z-score confidence interval parameter, which is set to 5 in our implementation. We then provide a comprehensive introduction to each component.

### 3.3. SaliencyCut

Ideally, the generated pseudo-anomalies are supposed to expand the distribution of known anomalies (e.g., Figure 4a) rather than be out of the distributed or mixed with real anomaly samples (e.g., Figure 4b,c).

To generate such desired pseudo-anomalies, the proposed SaliencyCut is directed by the saliency information. Since the saliency region of one sample reflects the model’s

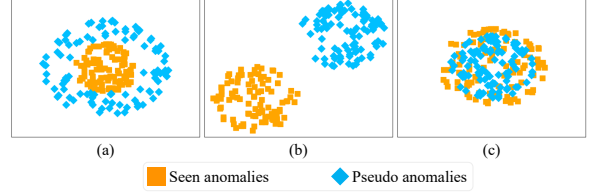


Figure 4. Illustration of distributions of seen anomalies and pseudo anomalies. (a) shows one ideal distribution of seen and pseudo anomalies, (b) and (c) are two less effective situations.

conclusive indication of its type, the non-saliency region of the normal sample can be regarded as the region where the network believes abnormal information may exist. To leverage this attribute of non-saliency regions to generate pseudo anomalies, the non-saliency region is pasted into another randomly selected normal sample in the corresponding location. Figure 5 provides an example of SaliencyCut.

Algorithm 1 presents the augmentation process of SaliencyCut,  $\odot$  represents element-wise multiplication in Line 5. To obtain saliency maps, we first input normal training samples and take the  $l_2$  norm of gradient values across input channels. The saliency maps are then downsampled to a grid size of  $g \times g$  and smoothed to the size of the input image using a B-spline 2D kernel matrix [18]. Elements of smoothed saliency map distribute continuously from 0 to 1. Setting a threshold value in the saliency maps yields a binary mask for isolating non-saliency regions. The threshold is a hyper-parameter that affects the size of non-saliency regions. Threshold selection is described in Section 4.8.

### 3.4. Two-Head Learning Mechanism

Since the generated pseudo-anomalies are well-expand but stay not too further from the distribution of seen anomalies, inspired by [7], we design a succinct two-head learning mechanism. Compared with the four-head learning mechanism [7], our learning mechanism is more concise yet more effective, as later verified both theoretically and empirically. Generally, normal knowledge can be seen as global features, hence we leverage one normal learning head consisting of a simple MLP structure to learn normal features. As the anomaly information often seems to be fine-grained features, we propose an anomaly learning head consisting of one patch-wise residual head (in Section 3.5) and one top- $K$  scoring module [27, 26] to extract anomaly knowledge in the high dimensional semantic space. Additionally, we present a theoretical interpretation of our two-head learning mechanism.

**Theoretical Support.** We aim to prove that our two-head learning mechanism offers a lower bound of data log-likelihood which is tighter compared to the multi-head learning approach [7]. Suggesting larger evidence, our two-head approach is thus in theory superior to multi-head in the

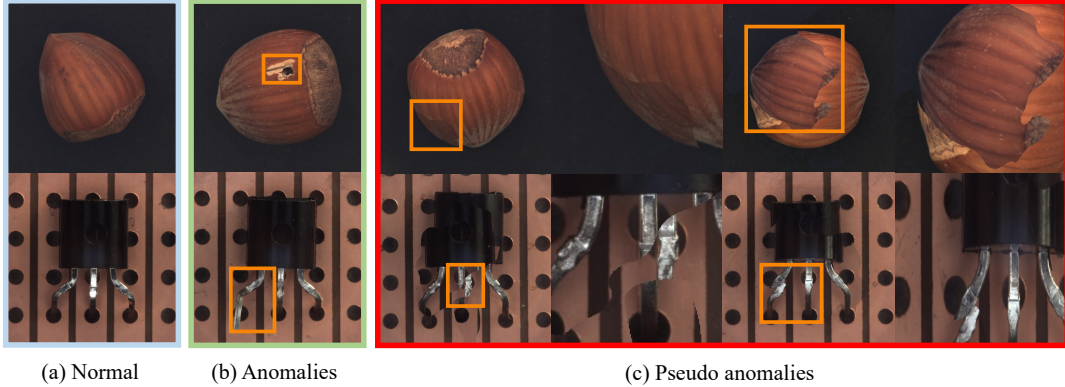


Figure 5. Visualization of normal samples, real anomaly samples and pseudo anomaly samples generated by SaliencyCut from Hazelnut and Transistor of MVTEC AD dataset [3]. (a) and (b) show normal and anomaly samples, respectively. Pseudo anomalies generated by SaliencyCut are presented in (c).

sense of maximum likelihood. Given a feature extraction network with parameters  $f(\cdot, \theta)$ , under the two-head learning paradigm, features of the normal instances  $x_i$ , anomaly instances  $x_j$  (including seen and pseudo) can be denoted as:

$$Z_i = f(x_i; \theta), i \in [1, n], \quad (3)$$

$$Q_j = f(x_j; \theta), j \in [n + 1, n + m], \quad (4)$$

where  $Z_i$  and  $Q_j$  are the extracted features of each normal and anomaly instance, respectively.

**Lemma 1:** Under the two-head learning paradigm, we aim to learn the scoring distribution of  $p(\phi|Z, Q)$ , the lower bound of the scoring distribution can be written as:

$$E_{p(z|\phi)}[\log p(\phi|Z, Q)] \geq E_{p(Z|\phi)}[\log p(Q|\phi) - \log p(Z|\phi)]. \quad (5)$$

**Lemma 2:** If the anomalies  $Q$  are divided into seen anomalies  $Q_s$  and pseudo anomalies  $A$ , and the scoring distribution is learned in a multi-head manner, the lower bound can be written as:

$$E_{p(z|\phi)}[\log p(\phi|Z, Q_s, A)] \geq E_{p(Z|\phi)}[\log p(A|\phi) + \log p(Q_s|\phi) - \log p(Z|\phi)]. \quad (6)$$

In the multi-head manner, since the pseudo anomaly instance is derived from normal samples,  $A$  can be considered independent of  $Q_s$ , then we have:

$$\begin{aligned} \log p(A|\phi) + \log p(Q_s|\phi) \\ = \log p(Q_s, A|\phi) \leq \log p(Q|\phi). \end{aligned} \quad (7)$$

Accordingly, our two-head learning mechanism has a tighter lower bound and is easier for optimization than the multi-head approach DRA [7], which offers theoretical justification for our method. Besides, our approach exhibits superior discriminative ability compared to DRA, as clearly shown in Figure 6. Later experiments confirm the advantages of our approach over multi-head approaches.

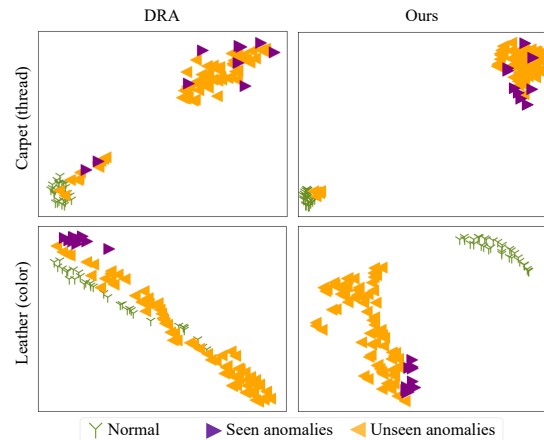


Figure 6. t-SNE visualization of features learned by DRA [7] and our approach during testing on two data subsets of MVTEC AD [3] (Leather and Carpet) under the hard setting. Thread and color are two seen anomaly types during training, respectively.

### 3.5. Patch-Wise Residual Module

We propose a patch-wise residual module for reliable learning of fine-grained anomalous knowledge by making residuals within the samples, which is motivated by two observations: 1) anomaly samples naturally contain both normal and abnormal features; 2) the residual features within one sample are more semantically uniform compared to that between anomalous and normal samples.

The patch-wise residual module consists of patch splitting and patch-wise subtraction. After obtaining feature maps from the backbone, we randomly split each feature map into several patches with the same size for residual learning, as shown in the Patch Residual Learning block of Figure 3. Since the location and size of the anomaly area are unknown, the size of each patch is supposed to be large enough to allow anomaly regions to be partitioned in the

spitted patches. Empirically, we set the patches’ size to half the size of the feature map, and one feature map is split into four different patches. Impact of patch number is described in Section 4.8. Patch-wise subtraction is performed within four split patches for residual learning as follows:

$$R = w_4 - (w_3 - (w_2 - w_1)), \quad (8)$$

where  $R$  denotes residual result and  $w_1, w_2, w_3$  and  $w_4$  are split patches. Patch-wise subtraction allows anomalous information to be highlighted in residual results, enabling the network to learn internal anomaly features within samples.

## 4. Experiments

### 4.1. Datasets

In experiments, we evaluate our method on six datasets with real anomalies: five industrial defect detection datasets include MVTec AD [3], SDD [40], AITEX [37], ELPV [6], and Optical [46], while one dataset Mastcam describes geological phenomena on Mars which regards particular geological features as anomalies [17].

### 4.2. Implementation Details

ResNet-18 [12] serves as the backbone network for feature learning. During training, the model is trained for 30 epochs, with 20 iterations per epoch and a batch size of 48, in which parameters are optimized by Adam. We empirically set the grid size  $g$  to 18 and the threshold for obtaining saliency masks to 0.4. The top- $K$  anomaly scoring approach is identical to that of DevNet [27, 26] and DRA [7] with  $K$  set to 10%. Area Under Receiver Operating Characteristic Curve (AUC-ROC) is utilized as the performance evaluation metric. All reported results are averaged over three independent trials.

Our model is compared to the four most related state-of-the-art supervised anomaly detection methods that use limited anomalies during training, including MLEP [22], DevNet [27, 26], DRA [7] and one ensemble method SAOE [7] (combining data augmentation-based Synthetic Anomalies [19, 23, 41] with Outlier Exposure [13, 31]). DevNet, MLEP and DRA also attempt to tackle the open-set fine-grained anomaly detection issue. SAOE performs data augmentation for pseudo anomalies generation and outlier exposure methods for anomaly detection, which is superior to utilizing one of these pseudo anomalies generation methods. The results of DevNet, MLEP, DRA and SAOE are obtained from DRA [7]. The results of three anomaly-free detection methods, KDAD [35], SSM [15] and CutPaste [19], are also from their papers.

### 4.3. Experimental Settings

**General Setting.** In the general setting of open-set fine-grained anomaly detection, a few anomalies randomly se-

lected from the test set are accessible during training, and the test set contains both seen anomalies and unseen anomalies or only seen anomalies. To measure the performance of the model with a few anomaly samples and very few anomaly samples, respectively, we set the general setting experiment with one training anomaly sample and ten training anomaly samples.

**Hard Setting.** In the hard setting, only one type of anomaly drawn from the test set is accessible during training, while the test set only contains unseen types of anomalies. Hard setting experiment is also set with one and ten anomaly training samples, respectively.

**Anomaly-Free Setting.** In the anomaly-free setting, there are no anomaly samples during training, the test set contains all types of anomalies.

### 4.4. Results under General Setting

The comparison results of different methods under the general setting are shown in Table 1.

**Ten Training Anomaly Samples.** Although the six datasets are derived from different scenarios, our approach achieves the best average AUC performance on five of them and the second-best results on MastCam. The upper block in Table 1 shows the performance at the level of data subsets, where our method outperforms other competitors in most cases. Our method achieves a boost of up to 4.4% compared to the second-best detector on Toothbrush.

**One Training Anomaly Sample.** By reducing the number of training anomaly samples from ten to one, the performance degradation of our method is significantly less than that of the other competitors. Our method obtains the best AUC results on all six datasets, with a maximum improvement of 21.9% compared to the second-best method on Capsule of MVTec AD. Meanwhile, our method achieves the smallest average AUC performance drop, with 11.4%, which is much better than DevNet (22.2%), MLEP (20.8%), SAOE (14.9%) and DRA (13.5%). On MVTec AD and Optical datasets, our average results trained with one anomaly sample significantly surpass some competitive methods trained with ten anomaly samples. In the more detailed results for data subsets of MVTec AD, our results trained with one anomaly outperforms all competitors trained with ten anomalies on Carpet, Grid, and Pill1. As the number of training anomaly samples decreases, our method suffers the least average AUC results reduction compared to the competing methods, evidencing the better generalization ability of our method.

### 4.5. Results under Hard Setting

Table 2 presents the comparison results on the five datasets under the hard setting.

**Ten Training Anomaly Samples.** Our method performs the best on all five datasets, improving mean AUC results

Table 1. AUC results (mean±std) on six real-world datasets under the general setting, with the best results **highlighted** and the second-best results underlined. The first fifteen datasets are data subsets of MVTec AD [3] whose results are averaged over these subsets.

Dataset	One Training Anomaly Sample					Ten Training Anomaly Samples				
	DevNet	MLEP	DRA	SAOE (ensemble)	Ours	DevNet	MLEP	DRA	SAOE (ensemble)	Ours
Carpet	0.746±0.076	0.701±0.091	<u>0.859±0.023</u>	0.766±0.098	<b>0.957±0.014</b>	0.867±0.040	0.781±0.049	<u>0.940±0.027</u>	0.755±0.136	<b>0.971±0.007</b>
Grid	0.891±0.040	0.839±0.028	<u>0.972±0.011</u>	0.921±0.032	<b>0.990±0.004</b>	0.967±0.021	0.980±0.009	<u>0.987±0.009</u>	0.952±0.011	<b>1.000±0.000</b>
Leather	0.873±0.026	0.781±0.020	0.989±0.005	<u>0.996±0.007</u>	<b>0.997±0.002</b>	<u>0.999±0.001</u>	0.813±0.158	<b>1.000±0.000</b>	<b>1.000±0.000</b>	<b>1.000±0.000</b>
Tile	0.752±0.038	0.927±0.036	<u>0.965±0.015</u>	0.935±0.034	<b>0.988±0.008</b>	0.987±0.005	0.988±0.009	<u>0.994±0.006</u>	0.944±0.013	<b>1.000±0.000</b>
Wood	0.900±0.068	0.660±0.142	<u>0.985±0.011</u>	0.948±0.009	<b>0.993±0.003</b>	<b>0.999±0.001</b>	<b>0.999±0.002</b>	<u>0.998±0.001</u>	0.976±0.031	0.998±0.001
Bottle	0.976±0.006	0.927±0.090	<b>1.000±0.000</b>	<u>0.989±0.019</u>	<b>1.000±0.000</b>	0.993±0.008	0.981±0.004	<b>1.000±0.000</b>	<u>0.998±0.003</u>	<b>1.000±0.000</b>
Capsule	0.564±0.032	0.558±0.075	<u>0.631±0.056</u>	0.611±0.109	<b>0.850±0.019</b>	0.865±0.057	0.818±0.063	<u>0.935±0.022</u>	0.850±0.054	<b>0.969±0.002</b>
Pill	0.769±0.017	0.656±0.061	<u>0.832±0.034</u>	0.652±0.078	<b>0.906±0.007</b>	0.866±0.038	0.845±0.048	<u>0.904±0.024</u>	0.872±0.049	<b>0.944±0.010</b>
Transistor	<u>0.722±0.032</u>	0.695±0.124	0.668±0.068	0.680±0.182	<b>0.754±0.015</b>	<u>0.924±0.027</u>	<b>0.927±0.043</b>	0.915±0.025	0.860±0.053	0.917±0.029
Zipper	0.922±0.018	0.856±0.086	<u>0.984±0.016</u>	0.970±0.033	<b>0.998±0.001</b>	0.990±0.009	0.965±0.002	<b>1.000±0.000</b>	0.995±0.004	<b>1.000±0.000</b>
Cable	0.783±0.058	0.688±0.017	<b>0.876±0.012</b>	0.819±0.060	<b>0.876±0.013</b>	0.892±0.020	0.857±0.062	<u>0.909±0.011</u>	0.862±0.022	<b>0.940±0.006</b>
Hazelnut	<u>0.979±0.010</u>	0.704±0.090	0.977±0.030	0.961±0.042	<b>0.987±0.005</b>	<b>1.000±0.000</b>	<b>1.000±0.000</b>	<b>1.000±0.000</b>	<b>1.000±0.000</b>	<b>1.000±0.000</b>
Metal_nut	0.876±0.007	0.878±0.038	<u>0.948±0.046</u>	0.922±0.033	<b>0.966±0.000</b>	0.991±0.006	0.974±0.009	<u>0.997±0.002</u>	0.976±0.013	<b>0.999±0.000</b>
Screw	0.399±0.187	0.675±0.294	<u>0.903±0.064</u>	0.653±0.074	<b>0.961±0.011</b>	0.970±0.015	0.899±0.039	<u>0.977±0.009</u>	0.975±0.023	<b>0.990±0.005</b>
Toothbrush	<b>0.753±0.027</b>	0.617±0.058	<u>0.650±0.029</u>	0.686±0.110	<u>0.752±0.009</u>	0.860±0.066	0.783±0.048	<u>0.826±0.021</u>	<u>0.865±0.062</u>	<b>0.909±0.005</b>
MVTec AD	0.794±0.014	0.744±0.019	<u>0.883±0.008</u>	0.834±0.007	<b>0.932±0.083</b>	0.945±0.004	0.907±0.005	<u>0.959±0.003</u>	0.926±0.010	<b>0.976±0.032</b>
Mastcam	0.595±0.016	0.625±0.045	<u>0.692±0.058</u>	0.662±0.018	<b>0.694±0.011</b>	0.790±0.021	0.798±0.026	<b>0.848±0.008</b>	0.810±0.029	<u>0.827±0.035</u>
SDD	<u>0.881±0.009</u>	0.811±0.045	0.859±0.014	0.781±0.009	<b>0.897±0.003</b>	<u>0.988±0.006</u>	0.983±0.013	<b>0.991±0.005</b>	0.955±0.020	<b>0.991±0.001</b>
ELPV	0.514±0.076	0.578±0.062	<u>0.675±0.024</u>	0.635±0.092	<b>0.699±0.051</b>	<u>0.846±0.022</u>	0.794±0.047	0.845±0.013	0.793±0.047	<b>0.852±0.005</b>
Optical	0.523±0.003	0.516±0.009	<u>0.888±0.012</u>	0.815±0.014	<b>0.895±0.009</b>	0.782±0.065	0.740±0.039	<b>0.965±0.006</b>	0.941±0.013	<b>0.965±0.001</b>
AITEX	0.598±0.070	0.564±0.055	<u>0.692±0.124</u>	0.675±0.094	<b>0.719±0.035</b>	0.887±0.013	0.867±0.037	<u>0.893±0.017</u>	0.874±0.024	<b>0.911±0.008</b>

Table 2. AUC results under the hard setting, where models are trained with one known anomaly type and tested to detect the rest of all other anomaly types. Each data subset is named by the known anomaly type.

Dataset	Data Subset	One Training Anomaly Sample					Ten Training Anomaly Samples				
		DevNet	MLEP	DRA	SAOE (ensemble)	Ours	DevNet	MLEP	DRA	SAOE (ensemble)	Ours
Carpet	Color	0.716±0.085	0.547±0.056	<u>0.879±0.021</u>	0.763±0.100	<b>0.932±0.019</b>	0.767±0.015	0.698±0.025	<u>0.886±0.042</u>	0.467±0.067	<b>0.951±0.005</b>
	Cut	0.666±0.035	0.658±0.056	<u>0.902±0.033</u>	0.664±0.165	<b>0.968±0.005</b>	0.819±0.037	0.653±0.120	<u>0.922±0.038</u>	0.793±0.175	<b>0.964±0.008</b>
	Hole	0.721±0.067	0.653±0.065	<u>0.901±0.033</u>	0.772±0.071	<b>0.967±0.005</b>	0.814±0.038	0.674±0.076	<u>0.947±0.016</u>	0.831±0.125	<b>0.961±0.004</b>
	Metal	0.819±0.032	0.706±0.047	<u>0.871±0.037</u>	0.780±0.172	<b>0.939±0.009</b>	0.863±0.022	0.764±0.061	<u>0.933±0.022</u>	0.883±0.043	<b>0.951±0.002</b>
	Thread	0.912±0.044	0.831±0.117	<u>0.950±0.029</u>	0.787±0.204	<b>0.994±0.001</b>	0.972±0.009	0.967±0.006	<u>0.989±0.004</u>	0.834±0.297	<b>0.998±0.000</b>
	Mean	0.767±0.018	0.679±0.029	<u>0.901±0.006</u>	0.753±0.055	<b>0.960±0.024</b>	0.847±0.017	0.751±0.023	<u>0.935±0.013</u>	0.762±0.073	<b>0.965±0.018</b>
Metal_nut	Bent	0.797±0.048	0.743±0.013	<u>0.952±0.020</u>	0.864±0.032	<b>0.976±0.012</b>	0.904±0.022	0.956±0.013	<u>0.990±0.003</u>	0.901±0.023	<b>0.996±0.003</b>
	Color	0.909±0.023	0.835±0.075	<u>0.946±0.023</u>	0.857±0.037	<b>0.967±0.019</b>	0.978±0.016	0.945±0.039	0.967±0.011	0.879±0.018	<b>0.979±0.004</b>
	Flip	0.764±0.014	0.813±0.031	<u>0.921±0.029</u>	0.751±0.090	<b>0.953±0.014</b>	<b>0.987±0.004</b>	0.805±0.057	0.913±0.021	0.795±0.062	<u>0.950±0.013</u>
	Scratch	<b>0.952±0.052</b>	0.907±0.085	0.909±0.023	0.792±0.075	<u>0.948±0.006</u>	<b>0.991±0.017</b>	0.805±0.153	0.911±0.034	0.845±0.041	<u>0.983±0.002</u>
		Mean	0.855±0.016	0.825±0.023	<u>0.932±0.017</u>	0.816±0.029	<b>0.961±0.017</b>	0.965±0.011	0.878±0.058	0.945±0.017	0.855±0.016
MastCam	Bedrock	0.495±0.028	0.532±0.036	<b>0.668±0.012</b>	<u>0.636±0.072</u>	0.626±0.037	0.550±0.053	0.512±0.062	<b>0.658±0.021</b>	<u>0.636±0.068</u>	0.581±0.054
	Broken-rock	0.533±0.020	0.544±0.088	0.645±0.053	<b>0.699±0.058</b>	<u>0.674±0.058</u>	0.547±0.018	0.651±0.063	0.649±0.047	<b>0.712±0.052</b>	<u>0.684±0.013</u>
	Drill-hole	0.555±0.037	0.636±0.066	0.657±0.070	<b>0.697±0.074</b>	<u>0.665±0.022</u>	0.583±0.022	0.660±0.002	0.725±0.005	0.682±0.042	<b>0.773±0.017</b>
	Drt	0.529±0.046	0.624±0.042	<u>0.713±0.053</u>	<b>0.735±0.020</b>	0.698±0.044	0.621±0.043	0.616±0.048	0.760±0.033	0.761±0.062	<b>0.796±0.028</b>
	Dump-pile	0.521±0.020	0.545±0.127	<u>0.767±0.043</u>	0.682±0.022	<b>0.775±0.020</b>	0.705±0.011	0.696±0.047	0.748±0.066	0.750±0.037	<b>0.773±0.053</b>
	Float	0.502±0.020	0.530±0.075	<u>0.670±0.065</u>	<b>0.711±0.041</b>	0.631±0.048	0.615±0.052	0.671±0.032	<b>0.744±0.073</b>	0.718±0.064	<u>0.735±0.007</u>
	Meteorite	0.467±0.049	0.476±0.014	0.637±0.015	0.669±0.037	<b>0.712±0.026</b>	0.554±0.021	0.473±0.047	<u>0.716±0.004</u>	0.647±0.030	<b>0.721±0.066</b>
	Scuff	0.472±0.031	0.492±0.037	0.549±0.027	<b>0.679±0.048</b>	<u>0.588±0.040</u>	0.588±0.034	0.504±0.052	0.636±0.086	<b>0.676±0.019</b>	0.607±0.021
	Veins	0.527±0.023	0.489±0.028	<b>0.699±0.045</b>	<u>0.688±0.069</u>	0.661±0.043	0.589±0.072	0.510±0.090	0.620±0.036	<b>0.686±0.053</b>	0.660±0.007
	Mean	0.511±0.013	0.541±0.007	0.667±0.012	<b>0.689±0.037</b>	<u>0.670±0.066</u>	0.588±0.011	0.588±0.016	0.695±0.004	<u>0.697±0.014</u>	<b>0.703±0.080</b>
ELPV	Mono	0.634±0.087	0.649±0.027	<b>0.735±0.031</b>	0.563±0.102	<u>0.720±0.054</u>	0.599±0.040	<b>0.756±0.045</b>	0.731±0.021	0.569±0.035	<u>0.735±0.020</u>
	Poly	0.662±0.050	0.483±0.247	<u>0.671±0.051</u>	0.665±0.173	<b>0.734±0.074</b>	<u>0.804±0.022</u>	0.734±0.078	0.800±0.064	0.796±0.084	<b>0.827±0.052</b>
		Mean	0.648±0.057	0.566±0.111	<u>0.703±0.022</u>	0.614±0.048	<b>0.727±0.065</b>	0.702±0.023	0.745±0.020	0.766±0.029	0.683±0.047
AITEX	Broken_end	0.712±0.069	0.441±0.111	0.708±0.094	<b>0.778±0.068</b>	<u>0.724±0.052</u>	0.658±0.111	<u>0.732±0.065</u>	0.693±0.099	0.712±0.068	<b>0.825±0.020</b>
	Broken_pick	0.552±0.003	0.476±0.070	<b>0.731±0.072</b>	0.644±0.039	<u>0.659±0.047</u>	0.585±0.028	0.555±0.027	<b>0.760±0.037</b>	0.629±0.012	<u>0.675±0.020</u>
	Cut_selvage	0.689±0.016	0.434±0.149	<u>0.739±0.101</u>	0.681±0.077	<b>0.790±0.048</b>	0.709±0.039	0.682±0.025	0.777±0.036	0.770±0.014	<b>0.856±0.009</b>
	Fuzzyball	0.617±0.075	0.525±0.157	<u>0.538±0.092</u>	0.650±0.064	<b>0.771±0.021</b>	0.734±0.039	0.677±0.223	<u>0.701±0.093</u>	0.842±0.026	<b>0.875±0.017</b>
	Nep	0.722±0.023	0.517±0.059	0.717±0.052	0.710±0.044	<b>0.731±0.019</b>	0.810±0.042	0.740±0.052	0.750±0.038	0.771±0.032	<b>0.908±0.008</b>
	Weft_crack	0.586±0.134	0.400±0.029	<u>0.669±0.045</u>	0.582±0.108	<b>0.686±0.013</b>	0.599±0.137	0.370±0.037	<b>0.717±0.072</b>	0.618±0.172	<u>0.697±0.014</u>
		Mean	0.646±0.034	0.466±0.030	<u>0.684±0.033</u>	0.674±0.034	<b>0.727±0.057</b>	0.683±0.032	0.626±0.041	0.733±0.009	0.724±0.032

by at least 0.6% compared to the best contestant. The maximum performance gain of 7.3% is achieved on AITEX, verifying the effectiveness of our method. Analysis at the data subsets level shows that our approach also achieves the best or the second-best detection performance in most cases.

**One Training Anomaly Sample.** Under the condition

of one training anomaly sample, our approach achieves the best performance on Carpet, Metal\_nut, AITEX, and ELPV, with the second-best results on MastCam. In regard to the mean performance on MastCam, the results of our methods are comparable to the ensemble method SAOE. Compared to the best contender, mean AUC performance increases by

Table 3. AUC results under the anomaly-free setting, all models are trained without anomaly samples.

Dataset	KDAD	SSM	CutPaste	Ours
Carpet	0.792±0.008	0.763	<u>0.939</u>	<b>0.984±0.011</b>
Grid	0.780±0.006	<b>1.000</b>	<b>1.000</b>	0.974±0.012
Leather	0.950±0.002	0.999	<b>1.000</b>	0.989±0.002
Tile	0.915±0.006	0.944	<u>0.946</u>	<b>0.981±0.008</b>
Wood	0.942±0.002	0.959	<u>0.991</u>	<b>0.997±0.002</b>
<b>Mean</b>	0.875±0.074	0.933±0.087	0.975±0.026	<b>0.985±0.011</b>

Table 4. Ablation study of our method and its variants.

Four-head learning	✓	-	-	-	-	
Two-head learning	-	✓	✓	✓	✓	
Latent residual	✓	✓	✓	-	-	
Patch-wise residual	-	-	-	✓	✓	
CutMix	✓	✓	-	-	-	
SaliencyCut	-	-	✓	✓	✓	
Carpet	Color	0.886±0.042	0.939±0.003	0.944±0.007	0.931±0.010	<b>0.951±0.005</b>
	Cut	0.922±0.038	0.940±0.005	0.955±0.002	0.961±0.006	<b>0.964±0.008</b>
	Hole	0.947±0.016	0.937±0.014	0.958±0.010	0.949±0.009	<b>0.961±0.004</b>
	Metal	0.933±0.022	0.938±0.008	0.948±0.006	0.948±0.016	<b>0.951±0.002</b>
	Thread	0.989±0.004	0.989±0.004	0.996±0.002	0.990±0.001	<b>0.998±0.000</b>
<b>Mean</b>	0.935±0.013	0.949±0.022	0.960±0.020	0.956±0.022	<b>0.965±0.018</b>	
Metal_nut	Bent	0.990±0.003	0.994±0.005	0.994±0.002	0.995±0.005	<b>0.996±0.003</b>
	Color	0.967±0.011	0.948±0.031	0.957±0.006	0.950±0.005	<b>0.979±0.004</b>
	Flip	0.913±0.021	0.944±0.005	0.901±0.018	<b>0.951±0.009</b>	0.950±0.013
	Scratch	0.911±0.034	0.967±0.012	0.974±0.004	0.975±0.009	<b>0.983±0.002</b>
	<b>Mean</b>	0.945±0.017	0.963±0.026	0.957±0.036	0.968±0.020	<b>0.977±0.018</b>

2.4%-5.9%. Compared to the scenarios with ten training anomaly samples, our method reduces AUC performance by an average of 3.68% on the five datasets, which is better than DRA (3.74%), MLEP (9.80%) and DevNet (7.16%), and close to SAOE (3.50%). Moreover, our model trained with one anomaly significantly exceeds competitive methods with ten anomalies on many of the data subsets as well as the datasets, such as DevNet, MLEP, DRA and SAOE on Carpet, its data subsets and Cur\_selvage of AITEX.

#### 4.6. Results under Anomaly-Free Setting

Table 3 presents the comparison results on the five texture datasets of MVTec AD under the anomaly-free scenario. Although there are no training anomaly samples, our approach can still work and shows better detection performance compared to the best recent anomaly-free detection methods, with an average AUC results improvement of 1% compared to the second best. This experiment demonstrates the effectiveness of SaliencyCut, which generates pseudo anomalies to promote the learning of unseen anomalies. At the dataset level, our method significantly outperforms other detectors on Carpet, Tile, and Wood, with the following best performance on Grid.

Compared to the competing methods under the general setting shown in Table 1, our model trained without anomaly samples is even better than other detectors training with ten anomaly samples, such as DevNet, MLEP, SAOE and DRA on Carpet, and DevNet and SAOE on Grid. This justifies the significantly better generalization ability of our method in detecting unseen anomaly samples.

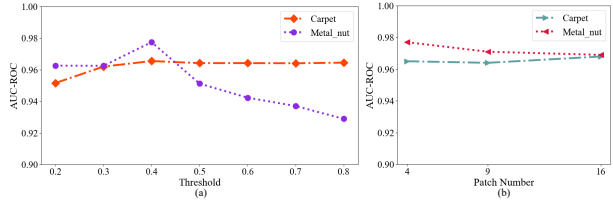


Figure 7. Sensitivity analysis of threshold (left) and patch number (right) on Carpet and Metal\_nut under the hard setting.

#### 4.7. Ablation Studies

Table 4 shows ablation study results under the hard setting on Carpet and Metal\_nut with ten training anomaly samples. We select DRA [7] as the baseline built with one four-head learning mechanism, one latent residual module, and CutMix augmentation. Compared to utilizing CutMix augmentation, SaliencyCut improves performance on two datasets by 0.9% on average under two-head learning and patch-wise residual paradigm, indicating its efficiency in detecting unseen anomaly samples.

Our two-head learning mechanism outperforms the four-head learning mechanism on various data subsets, particularly on Color of Carpet and Scratch of Metal\_nut, which demonstrates the effectiveness of the former approach and validates our theory. Replacing the latent residual module with the patch-wise residual module leads to further performance improvement on almost all data subsets and datasets. It verifies that the patch-wise residual allows the network to learn the discriminative features of anomalies.

#### 4.8. Sensitivity Analysis

**Threshold for Obtaining Saliency Masks.** Figure 7a shows AUC results with varying thresholds on Carpet and Metal\_nut under the hard setting. We successively set the threshold from 0.2 to 0.8 with a step size of 0.1 to analyse the sensitivity. When the threshold is set to 0.2, our method is able to generate effective pseudo-anomaly samples. As the threshold increases from 0.2 to 0.4, and the size of pasted non-saliency regions becomes smaller, our model obtains the best detection performance. With the increase of threshold, the size of non-saliency regions decreases, and the effectiveness of generated pseudo anomaly samples drops. Thus, the threshold is recommended to be set to 0.4 for producing suitable pseudo anomaly samples.

**Patch Number.** Figure 7b shows AUC results with varying patch number on Carpet and Metal\_nut under the hard setting. Our model shows less sensitivity to patch numbers, as all sizes deliver good performance.

### 5. Conclusion

We design a two-head learning mechanism with a patch-wise residual learning block, and a novel augmentation

method SaliencyCut guided by gradients to detect fine-grained anomalies in open-set scenarios. Extensive experiments under both general and hard settings evidence that our method overall outperforms the existing best methods. Additionally, our method can work under the anomaly-free setting and beat three anomaly-free detection models.

## References

- [1] Abhijit Bendale and Terrance E Boult. Towards Open Set Deep Networks. In *IEEE Conference on Computer Vision and Pattern Recognition (CVPR)*, pages 1563–1572, 2016. 1, 3
- [2] Liron Bergman and Yedid Hoshen. Classification-Based Anomaly Detection for General Data. In *International Conference on Learning Representations (ICLR)*, 2020. 3
- [3] Paul Bergmann, Michael Fauser, David Sattlegger, and Carsten Steger. MVTec AD—A Comprehensive Real-World Dataset for Unsupervised Anomaly Detection. In *IEEE Conference on Computer Vision and Pattern Recognition (CVPR)*, pages 9592–9600, 2019. 5, 6, 7
- [4] Raghavendra Chalapathy, Aditya Krishna Menon, and Sanjay Chawla. Anomaly Detection Using One-Class Neural Networks. *ArXiv*, abs/1802.06360, 2018. 3
- [5] Yuanhong Chen, Yu Tian, Guansong Pang, and Gustavo Carneiro. Deep One-Class Classification via Interpolated Gaussian Descriptor. In *Association for the Advancement of Artificial Intelligence (AAAI)*, pages 383–392, 2022. 3
- [6] Sergiu Deitsch, Vincent Christlein, Stephan Berger, Claudia Buerhop-Lutz, Andreas Maier, Florian Gallwitz, and Christian Riess. Automatic Classification of Defective Photovoltaic Module Cells in Electroluminescence Images. *Solar Energy*, 185:455–468, 2019. 6
- [7] Choubo Ding, Guansong Pang, and Chunhua Shen. Catching Both Gray and Black Swans: Open-Set Supervised Anomaly Detection. In *IEEE Conference on Computer Vision and Pattern Recognition (CVPR)*, pages 7378–7388, 2022. 1, 2, 3, 4, 5, 6, 8
- [8] Mariana-Iuliana Georgescu, Antonio Barbalau, Radu Tudor Ionescu, Fahad Shahbaz Khan, Marius Popescu, and Mubarak Shah. Anomaly Detection in Video via Self-Supervised and Multi-Task Learning. In *IEEE Conference on Computer Vision and Pattern Recognition (CVPR)*, pages 12742–12752, 2021. 3
- [9] Izhak Golan and Ran El-Yaniv. Deep Anomaly Detection Using Geometric Transformations. In *Annual Conference on Neural Information Processing Systems (NeurIPS)*, pages 9781–9791, 2018. 3
- [10] Dong Gong, Lingqiao Liu, Vuong Le, Budhaditya Saha, Moussa Reda Mansour, Svetha Venkatesh, and Anton van den Hengel. Memorizing Normality to Detect Anomaly: Memory-Augmented Deep Autoencoder for Unsupervised Anomaly Detection. In *IEEE International Conference on Computer Vision (ICCV)*, pages 1705–1714, 2019. 3
- [11] Nico Görnitz, Marius Kloft, Konrad Rieck, and Ulf Brefeld. Toward Supervised Anomaly Detection. *Journal of Artificial Intelligence Research*, 46:235–262, 2013. 3
- [12] Kaiming He, Xiangyu Zhang, Shaoqing Ren, and Jian Sun. Deep Residual Learning for Image Recognition. In *IEEE Conference on Computer Vision and Pattern Recognition (CVPR)*, pages 770–778, 2016. 6
- [13] Dan Hendrycks, Mantas Mazeika, and Thomas Dietterich. Deep Anomaly Detection with Outlier Exposure. In *International Conference on Learning Representations (ICLR)*, 2019. 6
- [14] Jinlei Hou, Yingying Zhang, Qiaoyong Zhong, Di Xie, Shiliang Pu, and Hong Zhou. Divide-and-Assemble: Learning Block-Wise Memory for Unsupervised Anomaly Detection. In *International Conference on Computer Vision (ICCV)*, pages 8771–8780, 2021. 3
- [15] Chaoqin Huang, Qinwei Xu, Yanfeng Wang, Yu Wang, and Ya Zhang. Self-Supervised Masking for Unsupervised Anomaly Detection and Localization. *IEEE Transactions on Multimedia*, 2022. 6
- [16] Rui Huang and Yixuan Li. Mos: Towards Scaling Out-of-Distribution Detection for Large Semantic Space. In *IEEE Conference on Computer Vision and Pattern Recognition (CVPR)*, pages 8706–8715, 2021. 3
- [17] Hannah R Kerner, Kiri L Wagstaff, Brian D Bue, Danika F Wellington, Samantha Jacob, Paul Horton, James F Bell, Chiman Kwan, and Heni Ben Amor. Comparison of Novelty Detection Methods for Multispectral Images in Rover-Based Planetary Exploration Missions. *Data Mining and Knowledge Discovery*, 34(6):1642–1675, 2020. 6
- [18] ETY Lee. A Simplified B-Spline Computation Routine. *Computing*, 29(4):365–371, 1982. 4
- [19] Chun-Liang Li, Kihyuk Sohn, Jinsung Yoon, and Tomas Pfister. Cutpaste: Self-Supervised Learning for Anomaly Detection and Localization. In *IEEE Conference on Computer Vision and Pattern Recognition (CVPR)*, pages 9664–9674, 2021. 1, 2, 3, 6
- [20] Ziqian Lin, Sreya Dutta Roy, and Yixuan Li. Mood: Multi-Level Out-of-Distribution Detection. In *IEEE Conference on Computer Vision and Pattern Recognition (CVPR)*, pages 15313–15323, 2021. 3
- [21] Si Liu, Rishiek Garrepalli, Thomas Dietterich, Alan Fern, and Dan Hendrycks. Open Category Detection with PAC Guarantees. In *International Conference on Machine Learning (ICML)*, pages 3169–3178, 2018. 1, 3
- [22] Wen Liu, Weixin Luo, Zhengxin Li, Peilin Zhao, Shenghua Gao, et al. Margin Learning Embedded Prediction for Video Anomaly Detection with A Few Anomalies. In *International Joint Conference on Artificial Intelligence (IJCAI)*, pages 3023–3030, 2019. 3, 6
- [23] Philipp Liznerski, Lukas Ruff, Robert A Vandermeulen, Billy Joe Franks, Marius Kloft, and Klaus-Robert Müller. Explainable Deep One-Class Classification. In *International Conference on Learning Representations (ICLR)*, 2021. 6
- [24] Avery Ma, Nikita Dvornik, Ran Zhang, Leila Pishdad, Konstantinos G. Derpanis, and Afsaneh Fazly. SAGE: Saliency-Guided Mixup with Optimal Rearrangements. In *British Machine Vision Conference (BMVC)*, 2022. 3
- [25] Guansong Pang, Longbing Cao, Ling Chen, and Huan Liu. Learning Representations of Ultrahigh-Dimensional Data for

- Random Distance-Based Outlier Detection. In *International Conference on Knowledge Discovery and Data Mining (KDD)*, pages 2041–2050, 2018. 3
- [26] Guansong Pang, Choubao Ding, Chunhua Shen, and Anton van den Hengel. Explainable Deep Few-Shot Anomaly Detection with Deviation Networks. *ArXiv*, abs/2108.00462, 2021. 1, 3, 4, 6
- [27] Guansong Pang, Chunhua Shen, and Anton van den Hengel. Deep Anomaly Detection with Deviation Networks. In *International Conference on Knowledge Discovery and Data Mining (KDD)*, pages 353–362, 2019. 1, 3, 4, 6
- [28] Hyunjong Park, Jongyoun Noh, and Bumsub Ham. Learning Memory-Guided Normality for Anomaly Detection. In *IEEE Conference on Computer Vision and Pattern Recognition (CVPR)*, pages 14360–14369, 2020. 3
- [29] Pramuditha Perera, Ramesh Nallapati, and Bing Xiang. Ogan: One-Class Novelty Detection Using GANs with Constrained Latent Representations. In *IEEE Conference on Computer Vision and Pattern Recognition (CVPR)*, pages 2898–2906, 2019. 3
- [30] Pramuditha Perera and Vishal M Patel. Learning Deep Features for One-Class Classification. *IEEE Transactions on Image Processing*, 28(11):5450–5463, 2019. 3
- [31] Tal Reiss, Niv Cohen, Liron Bergman, and Yedid Hoshen. Panda: Adapting Pretrained Features for Anomaly Detection and Segmentation. In *IEEE Conference on Computer Vision and Pattern Recognition (CVPR)*, pages 2806–2814, 2021. 6
- [32] Lukas Ruff, Robert Vandermeulen, Nico Goernitz, Lucas Deecke, Shoaib Ahmed Siddiqui, Alexander Binder, Emmanuel Müller, and Marius Kloft. Deep One-Class Classification. In *International Conference on Machine Learning (ICML)*, pages 4390–4399, 2018. 3
- [33] Lukas Ruff, Robert A Vandermeulen, Nico Görnitz, Alexander Binder, Emmanuel Müller, Klaus-Robert Müller, and Marius Kloft. Deep Semi-Supervised Anomaly Detection. In *International Conference on Learning Representations (ICLR)*, 2020. 3
- [34] Mohammad Sabokrou, Mohammad Khalooei, Mahmood Fathy, and Ehsan Adeli. Adversarially Learned One-Class Classifier for Novelty Detection. In *IEEE Conference on Computer Vision and Pattern Recognition (CVPR)*, pages 3379–3388, 2018. 3
- [35] Mohammadreza Salehi, Niousha Sadjadi, Soroosh Baselizadeh, Mohammad H Rohban, and Hamid R Rabiee. Multiresolution Knowledge Distillation for Anomaly Detection. In *IEEE Conference on Computer Vision and Pattern Recognition (CVPR)*, pages 14902–14912, 2021. 6
- [36] Thomas Schlegl, Philipp Seeböck, Sebastian M Waldstein, Georg Langs, and Ursula Schmidt-Erfurth. F-AnoGAN: Fast Unsupervised Anomaly Detection with Generative Adversarial Networks. *Medical Image Analysis*, 54:30–44, 2019. 3
- [37] Javier Silvestre-Blanes, Teresa Albero Albero, Ignacio Miralles, Rubén Pérez-Llorens, and Jorge Moreno. A Public Fabric Database for Defect Detection Methods and Results. *Autex Research Journal*, 19(4):363–374, 2019. 6
- [38] Kihyuk Sohn, Chun-Liang Li, Jinsung Yoon, Minh Jin, and Tomas Pfister. Learning and Evaluating Representations for Deep One-Class Classification. In *International Conference on Learning Representations (ICLR)*, 2021. 3
- [39] Yiyu Sun, Yifei Ming, Xiaojin Zhu, and Yixuan Li. Out-of-Distribution Detection with Deep Nearest Neighbors. In *International Conference on Machine Learning (ICML)*, pages 20827–20840, 2022. 1, 3
- [40] Domen Tabernik, Samo Šela, Jure Skvarč, and Danijel Skočaj. Segmentation-Based Deep-Learning Approach for Surface-Defect Detection. *Journal of Intelligent Manufacturing*, 31(3):759–776, 2020. 6
- [41] Jihoon Tack, Sangwoo Mo, Jongheon Jeong, and Jinwoo Shin. Csi: Novelty Detection via Contrastive Learning on Distributionally Shifted Instances. In *Annual Conference on Neural Information Processing Systems (NeurIPS)*, pages 11839–11852, 2020. 6
- [42] Yu Tian, Guansong Pang, Fengbei Liu, Yuanhong Chen, Seon Ho Shin, Johan W Verjans, Rajvinder Singh, and Gustavo Carneiro. Constrained Contrastive Distribution Learning for Unsupervised Anomaly Detection and Localisation in Medical Images. In *International Conference on Medical Image Computing and Computer Assisted Intervention (MICCAI)*, pages 128–140, 2021. 3
- [43] AFM Uddin, Mst Monira, Wheemyung Shin, TaeChoong Chung, Sung-Ho Bae, et al. Saliencymix: A Saliency Guided Data Augmentation Strategy for Better Regularization. In *International Conference on Learning Representations (ICLR)*, 2021. 3
- [44] Sagar Vaze, Kai Han, Andrea Vedaldi, and Andrew Zisserman. Generalized Category Discovery. In *IEEE Conference on Computer Vision and Pattern Recognition (CVPR)*, pages 7492–7501, 2022. 1, 3
- [45] Siqi Wang, Yijie Zeng, Xinwang Liu, En Zhu, Jianping Yin, Chuanfu Xu, and Marius Kloft. Effective End-to-end Unsupervised Outlier Detection via Inlier Priority of Discriminative Network. In *Annual Conference on Neural Information Processing Systems (NeurIPS)*, pages 5960–5973, 2019. 3
- [46] Matthias Wieler and Tobias Hahn. Weakly Supervised Learning for Industrial Optical Inspection. In *DAGM Symposium*, 2007. 6
- [47] Zhongqi Yue, Tan Wang, Hanwang Zhang, Qianru Sun, and Xiansheng Hua. Counterfactual Zero-Shot and Open-Set Visual Recognition. In *IEEE Conference on Computer Vision and Pattern Recognition (CVPR)*, pages 15399–15409, 2021. 3
- [48] Sangdoon Yun, Dongyoon Han, Seong Joon Oh, Sanghyuk Chun, Junsuk Choe, and Youngjoon Yoo. Cutmix: Regularization strategy to train strong classifiers with localizable features. In *IEEE International Conference on Computer Vision (ICCV)*, pages 6022–6031, 2019. 1, 2, 3
- [49] Alireza Zaeemzadeh, Niccolo Bisagno, Zeno Sambugaro, Nicola Conci, Nazanin Rahnavard, and Mubarak Shah. Out-of-Distribution Detection Using Union of 1-Dimensional Subspaces. In *IEEE Conference on Computer Vision and Pattern Recognition (CVPR)*, pages 9452–9461, 2021. 1, 3
- [50] Muhammad Zaigham Zaheer, Jin-ha Lee, Marcella Astrid, and Seung-Ik Lee. Old is Gold: Redefining the Adversarially Learned One-Class Classifier Training Paradigm. In

- IEEE Conference on Computer Vision and Pattern Recognition (CVPR)*, pages 14171–14181, 2020. 3
- [51] Hongyi Zhang, Moustapha Cisse, Yann N Dauphin, and David Lopez-Paz. Mixup: Beyond Empirical Risk Minimization. In *International Conference on Learning Representations (ICLR)*, 2018. 3
- [52] Jianpeng Zhang, Yutong Xie, Guansong Pang, Zhibin Liao, Johan Verjans, Wenxing Li, Zongji Sun, Jian He, Yi Li, Chunhua Shen, et al. Viral Pneumonia Screening on Chest X-Rays Using Confidence-Aware Anomaly Detection. *IEEE Transactions on Medical Imaging*, 40(3):879–890, 2020. 3
- [53] Chong Zhou and Randy C Paffenroth. Anomaly Detection with Robust Deep Autoencoders. In *International Conference on Knowledge Discovery and Data Mining (KDD)*, pages 665–674, 2017. 3
- [54] Da-Wei Zhou, Han-Jia Ye, and De chuan Zhan. Learning Placeholders for Open-Set Recognition. In *IEEE Conference on Computer Vision and Pattern Recognition (CVPR)*, pages 4399–4408, 2021. 3
- [55] Kang Zhou, Yuting Xiao, Jianlong Yang, Jun Cheng, Wen Liu, Weixin Luo, Zaiwang Gu, Jiang Liu, and Shenghua Gao. Encoding Structure-Texture Relation with P-Net for Anomaly Detection in Retinal Images. In *European Conference on Computer Vision (ECCV)*, pages 360–377, 2020. 3